Shear zone folds: records of flow perturbation or structural inheritance?

G. I. ALSOP[1] & R. E. HOLDSWORTH[2]
[1]*Crustal Geodynamics Group, School of Geography & Geosciences, University of St Andrews, St Andrews, Fife, Scotland KY16 9AL, UK (e-mail: gia@st-andrews.ac.uk)*
[2]*Reactivation Research Group, Department of Earth Sciences, University of Durham, Durham, DH1 3LE, UK*

Abstract: Deformation within shear zones can be both temporally and spatially variable, resulting in multiple generations of folds which display a range of scales and overprinting relationships in mylonitic rocks associated with high strain zones. Despite such complexities, two main fold associations are broadly recognized in many shear zone settings: early tight to isoclinal sheath folds, often with mylonitic limbs that are post-dated by one or more local generations of synshearing folds which are preserved within, or root downwards into mylonitic high strain zones. These latter structures locally fold the mylonitic foliation and lineation whilst displaying geometric characteristics that are kinematically compatible with the movement regime of the major shear zone. Using examples related to ductile thrusting in Moine metasediments of north Scotland, we show that both types of fold display predictable geometric patterns on fabric topology plots. Fold axes and axial surfaces display consistent changes in asymmetry and sense of obliquity relative to local, transport-parallel mineral lineations that can be used to map out a series of culminations and depression zones. The sheath folds preserve more acute, but almost identical geometric patterns compared to the later synshearing folds, with culmination and depression zones often coinciding in location and scale. Detailed analysis also demonstrates that the distribution of finite strain is systematically linked to the architecture of all folds and that clear and predictable relationships exist between the fabric topologies of both the sheath folds and synshearing folds. These consistent topological relationships could be explained in terms of a *fold evolution model*, where sheath folds represent a more highly deformed and evolved variety of synshearing folds originally generated during perturbations in ductile flow. However, an alternative *fold inheritance model* predicts that the gross structural architecture generated during sheath folding may subsequently control the geometry and govern the orientation of the synshearing folds. Both models may be widely applicable in a broad range of shear zone environments.

Within orogenic systems, there is a close association between folding and localized zones of enhanced ductile deformation forming shear zones. This relationship has been studied by generations of geologists working on a variety of scales and tectono-metamorphic environments. Although a broad link between both contractional and extensional shear zones and folding is well established (e.g. see Harris *et al.* 2002 for a review), precise geometrical relationships between planar and linear shear zone fabrics with fold morphologies is the subject of much past and current research (e.g. Ramsay 1967; Hansen 1971; Coney 1974; Ramsay 1979; Fossen & Rykkelid 1990; Dillon *et al.* 1990; Carreras 1997; Bolhar & Ring 2001). In particular, the role of folding with respect to the timing of shear zone development and progressive deformation within mylonites, together with the kinematic interpretation of folding are the foci of continuing research (e.g. Fletcher & Bartley 1994; Ez 2000; Ramsay & Lisle 2000). This study concentrates on the evolution of shear zone-related folding and in particular the generation of synshearing flow folds, together with those modified by progressive shear culminating in the development of sheath folds (Fig. 1).

Two broad fold associations are typically recognized within shear zones. First, an early phase of tight to isoclinal, highly curvilinear folds with mylonitic limbs and 'low-strain' hinges which may be cross-cut at low angles by broader zones of high strain such as ductile thrusts (e.g. Carreras *et al.* 1977; Quinquis *et al.* 1978; Minigh 1979; Cobbold & Quinquis 1980; Berthé & Brun 1980; Henderson 1981; Lacassin & Mattauer 1985; Holdsworth 1989). Models of sheath folding are classically applied to such

From: ALSOP, G. I., HOLDSWORTH, R. E., MCCAFFREY, K. J. W. & HAND, M. (eds) 2004. *Flow Processes in Faults and Shear Zones*. Geological Society, London, Special Publications, **224**, 177–199. 0305-8719/$15.00

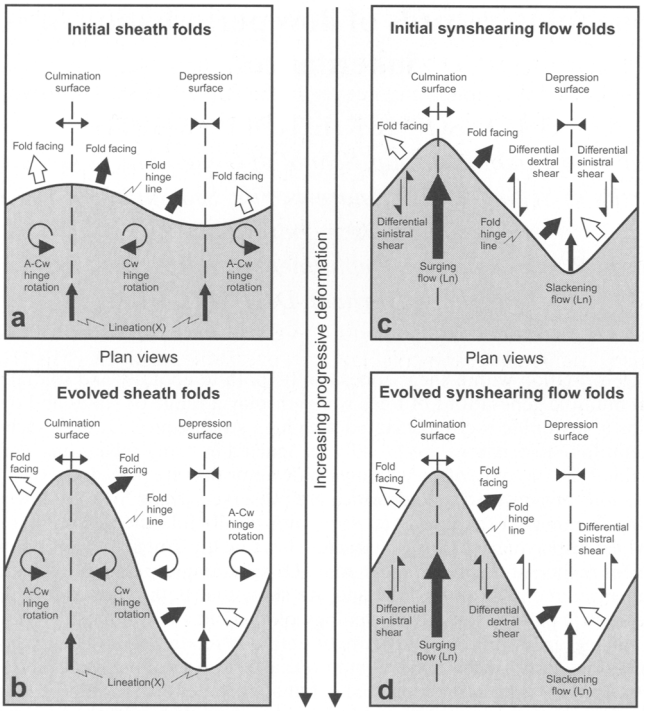

Fig. 1. Summary schematic diagrams illustrating increasing deformation and evolution of fold hinge-lines associated with sheath folds (**a**,**b**) and synshearing flow folds (**c**,**d**). Diagrams are plan view and show clockwise (Cw) and anticlockwise (A-Cw) rotations of fold hinge-lines which are marked by reversals in fold facing directions about the transport-parallel culmination and depression surfaces. Synshearing flow folds are generated by surging flow (large transport (Ln) arrow) and slackening flow (small transport (Ln) arrow) separated by differential sinistral and dextral shear. See text for further details.

folds (see Alsop & Holdsworth 1999 for a review) (Fig. 1a,b). Secondly, one or more generations of later, synshearing folds occur, which are temporally, spatially and kinematically related to the shear zones (e.g. Carreras *et al.* 1977; Bell 1978; Cobbold & Quinquis 1980; Evans & White 1984; Ridley 1986; Holdsworth 1990). Models of flow perturbation folding may be applied to these folds (see Alsop & Holdsworth 2002 for a review) (Fig. 1c,d). The analysis of consistent and ordered scale-independent relationships between the transport direction and fold hinges, fold asymmetries and axial surfaces can provide a record of shear zone evolution within a broad range of coherent kinematic systems. Following a brief summary of both sheath and synshearing flow folding, details of a case study from north Scotland are presented which examines the sequential fabric relationships that exist between such evolving fold systems.

Sheath folds

Sheath folds are defined here as folds in which high strain has been superimposed on the original fold geometry so that the hinges now display a curvature in excess of 90° (see also Ramsay & Huber 1987 p. 311) (Fig. 1a,b). Sheath folds may be further subdivided into tongue folds with a hinge line curvature between 90°–160° and tubular folds with a hairpin-like curvature above 160° (Skjernaa 1989). The subparallelism of large segments of curvilinear hinge-lines with the mineral elongation lineation (X) in high strain settings may be achieved via a variety of mechanisms. Accepted traditional explanations for co-linearity of hinges and mineral lineations assume bulk simple shear or plane strain non-coaxial flow in which fold hinges rotate (typically with associated interlimb tightening) towards the transport-parallel mineral lineation (X) during intense ductile

shearing (Bryant & Read 1969; Sanderson 1973; Escher & Watterson 1974; Rhodes & Gayer 1977; Bell 1978; Williams 1978; Mies 1991) (Fig. 1a,b). In such flow regimes, folds that are generated oblique to transport will display unidirectional rotation with all hinges rotating in the same (clockwise or anticlockwise) sense which is determined by the initial sense of hinge-transport obliquity. This results in asymmetric, typically tight-isoclinal cylindrical folds which, due to incomplete rotation, frequently preserve a small angle of obliquity to the transport lineation (see Alsop 1992). Fold hinges which initiate broadly orthogonal to shear may display reversals in the sense of hinge/lineation obliquity along their length, reflecting the initial growth and lateral propagation of the buckle fold hinge (Fig. 1a). Such mildly curvilinear hinges may subsequently undergo opposing senses of relative rotation resulting in extremely curvilinear sheath fold forms. Opposing senses of (clockwise and anticlockwise) rotation result in reversals in the polarity of minor fold facing which is directed outwards away from upwards-closing antiformal culminations and inwards towards downwards-closing synformal depressions (e.g. Holdsworth 1988; Alsop & Holdsworth 1999) (Fig. 1b). Originally consistent buckle fold geometries which undergo opposing rotations at opposite ends will display either a S or Z down-plunge asymmetry depending on the sense of rotation, thus resulting in double-vergence geometries along the length of the individual hinge (e.g. Hobbs *et al.* 1976 p. 168; Holdsworth & Roberts 1984; Alsop & Holdsworth 1999). Reversals in vergence and the polarity of minor fold facing therefore mark transport-parallel and foliation-normal culmination/depression (medial) surfaces which bisect the resulting curvilinear hinge closures (Fig. 1b; Alsop & Holdsworth 1999). Thus, progressive ductile shearing is considered to result in the modification and *rotation* of originally high-angle, gently curved fold hinges towards the transport direction. An alternative mechanism in which synshearing fold geometries *initiate* at variable angles to transport as a consequence of perturbations in ductile flow within shear zones will now be considered.

Synshearing flow folds

Curvilinear fold patterns may be generated adjacent to shear zones via variations in the relative rate of ductile flow. Temporal and spatial variations in the shear strain rate can result in localized perturbations in flow which may involve acceleration (surging flow) or deceleration (slackening flow) with respect to the adjacent flow (see Coward & Potts 1983; Platt 1983; Ridley 1986; Holdsworth 1990; Alsop & Holdsworth 1993, 2002; Alsop *et al.* 1996). Surging flow results in overall contraction at the front of the deformation cell resulting in folding and the development of transport-parallel and foliation-normal culmination surfaces which bisect the cell (Fig. 1c; Alsop & Holdsworth 2002). Conversely, slackening flow leads to a mirror image configuration with contraction and thickening at the rear of the cell associated with depression surfaces (Fig. 1c). On the lateral flanks of flow perturbation cells, S folds (viewed down-plunge) are developed anticlockwise of the mineral lineation during differential dextral shear, whereas Z folds are produced by differential sinistral shear (Fig. 1d; Coward & Potts 1983; Alsop & Holdsworth 1993).

Although analysis of synshearing folds may provide evidence of the scale and nature of heterogeneous flow and deformation cells in shear zones (e.g. Alsop *et al.* 1996), many uncertainties still exist. Although flow perturbations represent a plausible model to explain the generation of variably orientated synshearing folds, questions remain as to what extent the attitude of the pre-existing structures within the mylonite may influence the geometry and orientation of such folds. Clearly, variably orientated layering which is oblique to the strain ellipsoid will inherently create a range of possible fold orientations (e.g. Flinn 1962; Treagus & Treagus 1981: Carreras 1997). In order to address these issues, a detailed case study of curvilinear sheath folds and variably orientated synshearing folds from the Caledonides of north Scotland is described (Fig. 2).

Regional setting; Caledonian Moine Nappe, Sutherland

The regional geology of NW Scotland is dominated by structures generated during the Lower Palaeozoic Caledonian orogeny (*c.* 460–420 Ma), the most important of which are the ESE-dipping Moine Thrust and overlying Sgurr Beag/Naver Thrust (Fig. 2). In Sutherland, these thrusts, which underlie the Moine and Naver Nappes respectively, formed as a result of major west to NW-directed thrusting. The Moine Thrust separates imbricated, essentially unmetamorphosed sedimentary sequences overlying Precambrian metamorphic basement of the Lewisian complex (western foreland)

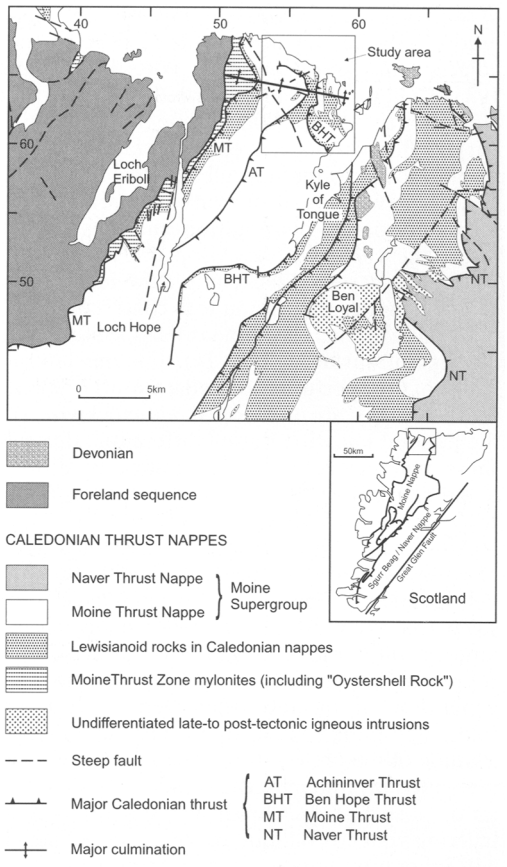

Fig. 2. Simplified geological map of the Moine and Naver Nappes in the Kyle of Tongue area highlighting the location of the study area (see also British Geological Survey 1997, 2002). Major NW-to-WNW-directed Caledonian ductile thrusts which carry reworked Lewisian in the hanging wall are shown with solid barbs. The reference grid relates to the UK National Grid with the map area falling within the NC prefix quadrangle. The inset shows the location of the map in relation to Scotland with the Moine and Naver Nappes being carried on Caledonian thrusts.

from metamorphosed Neoproterozoic psammites and pelites forming the Moine Nappe. Further east the Naver Thrust juxtaposes migmatized (in the hanging wall) and non-migmatized Moine psammites. Within both the Moine and Naver Nappes, psammites and subordinate pelites of the Moine Supergroup are tectonically interleaved with high grade, Lewisian-like basement upon which the Moine is thought to have been unconformably deposited (Holdsworth 1989). Tectonic repetition is generated by Caledonian-age ductile thrusting and folding that forms the main (D_2) fabrics observed throughout the region. These Caledonian structures, which are the focus of the present study, consistently overprint earlier D_1 fabrics and associated metamorphic assemblages considered to be of Neoproterozoic age (Holdsworth 1989).

Regional D_2 deformation has resulted in a gently east-dipping, approximately bedding-parallel foliation (Sn) which intensifies into broad zones of platy mylonite that define Caledonian ductile thrusts formed at mid-crustal depths (greenschist–amphibolite facies) (see Holdsworth *et al.* 2001 and references therein). Within the plane of the foliation, a pronounced mineral lineation (Ln) defined by aligned micas and elongate quartz – feldspar aggregates plunges gently towards the east directly down the dip of the foliation. This is considered by most authors to represent the trend of tectonic transport within a regime of non-coaxial flow associated with bulk plane strain (Holdsworth & Grant 1990). D_2 deformation has resulted in two generations of folding (termed F_2 and F_3) which show distinct and consistent relationships to the regional foliations and lineations. F_2 folds of bedding display an axial planar foliation and are marked by highly curvilinear hinge-line patterns on all scales that have been interpreted previously in terms of sheath fold models (e.g. Holdsworth 1987, 1989, 1990; Alsop & Holdsworth 1999). F_3 folds of the regional foliation and lineation are spatially associated with the D_2 ductile thrust zones, and display axial traces that vary between transport parallel and transport normal. Such folds are developed in both the Moine and Naver Nappes (e.g. Holdsworth 1990; Alsop & Holdsworth 1993; Alsop *et al.* 1996) and have been previously interpreted in terms of flow perturbation models (e.g. Alsop & Holdsworth 2002).

Detailed geometric analyses of the F_2 sheath folding and F_3 flow perturbation folding have been documented previously from the region in separate publications (Alsop & Holdsworth 1993, 1999, 2002). This study presents the first quantitative analysis of the relationships and associations that exist between F_2 and F_3 structures in a well-exposed region of the Moine Nappe (Figs 2 & 3). Similarities and differences between these folds will be described prior to a discussion on the origins of folding in terms of *fold evolution models* associated with long-lived flow perturbations in ductile mylonites and *fold inheritance models* governed by inherited structural architecture.

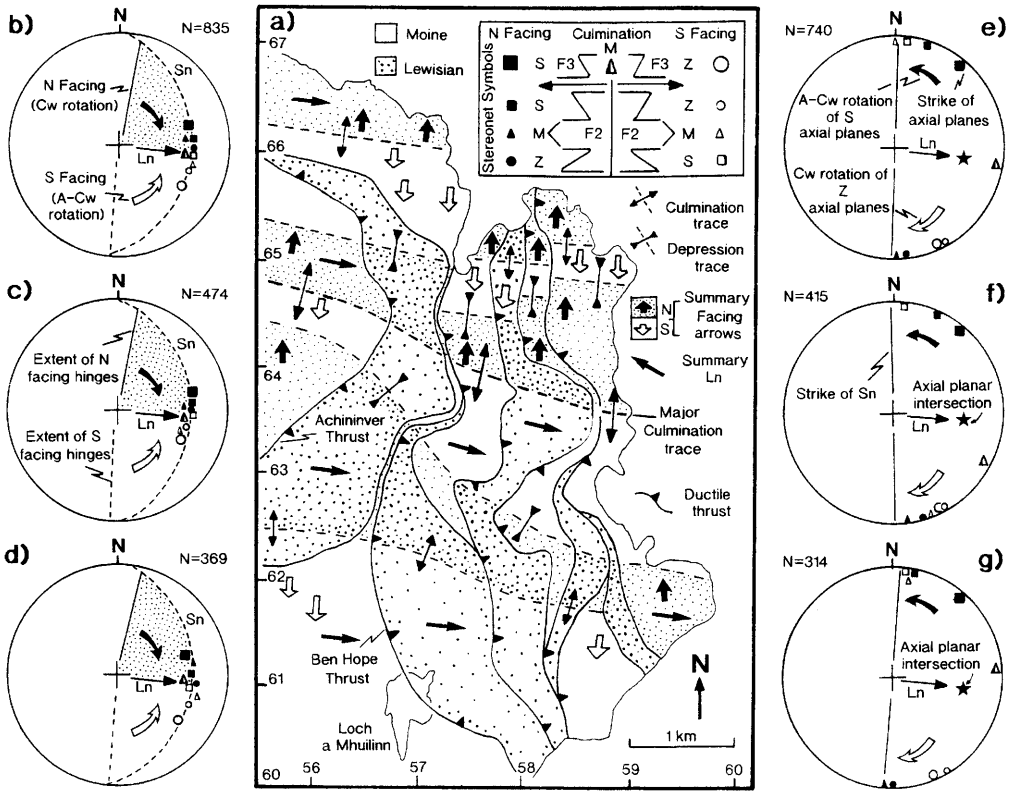

Fig. 3. (**a**) Simplified structural map of the study area highlighting the location of ductile thrusts and a major WNW-trending culmination trace which divides the region in to northern and southern subareas. Summary facing domains (based on younging evidence) are highlighted in close stipple. When viewed down-plunge, culmination and depression surfaces are offset in a consistent sinistral (top-to-the-north) sense by D_2 ductile thrusts located along pelitic units, suggesting strain localization and continued progressive deformation within these weaker horizons. Detailed structural analysis within Lewisian and Moine rocks of the study area illustrate the vergence and facing relationships of minor folds, together with the relative obliquity between fold hinges and the Ln mineral lineation. The inset key shows the relative structural position of schematic (F_3) flow folds (larger symbols on upper row) and (F_2) sheath folds together with stereonet symbols. Equal area lower hemisphere stereographic projections of all fold hinges (**b**) subdivided into northern (**c**) and southern (**d**) domains clearly show clockwise rotation of north-facing hinges (stipple) and anticlockwise rotation of south-facing folds. Poles to all associated axial planes (**e**) subdivided into northern (**f**) and southern (**g**) domains clearly show anticlockwise rotation of S axial planes and clockwise rotation of Z axial planes towards the mean strike of the regional (Sn) foliation. Note that the intersection of the great circles representing the mean Z and S axial planes (starred) is typically parallel to the transport lineation (Ln). Solid and open symbols represent north-facing and south-facing structures respectively. Refer to Fig. 2 for location and text for further details.

The Melness folds case study

The Melness area to the west of the Kyle of Tongue is an ideal place to compare and contrast sheath and synshearing folds as it contains diverse lithologies interlayered on all scales which encourages the development of folds. In addition, it is well exposed and readily accessible. Structurally, the Melness area is dominated by a Caledonian ductile thrust stack associated with top-to-the-WNW shear criteria including the Achininver and Ben Hope thrusts which collectively form the Talmine Imbricate Zone (Holdsworth *et al.* 2001) (Figs 2 & 3a). The ductile thrusts have been openly folded by kilometre-scale folds which are predominantly parallel to the WNW-trend of tectonic transport and separate north and south facing domains. These upright folds define culmination/depression surfaces which root downwards onto

underlying thrusts and have previously been attributed to perturbations in ductile flow within the thrust-related mylonitic shear zones (Holdsworth 1990; Alsop & Holdsworth 1993, 2002; Alsop *et al.* 1996) (Figs 2 & 3a).

Major culmination surfaces are orthogonal to the regional foliation surface and parallel to the transport direction marked by the mineral lineation. The largest WNW–ESE trending culmination surface in the study area intersects the gently east-dipping form of the detachment directly beneath the Moine Thrust Zone mylonites (Figs 2 & 3a). The planar geometry of this structure in the hinge of the culmination suggests that it has not been affected by the synshearing flow folding and has acted as the local basal décollement to the deformation (Alsop *et al.* 1996; Holdsworth *et al.* 2001 Alsop & Holdsworth 2002). Thus, the Melness study area is marked by a major culmination, which together with the presence of earlier F_2 antiformal sheath folds cored by Lewisianoid inliers results in a dome-dominated structural setting (see Alsop & Holdsworth 1999, 2002 for further details). Detailed descriptions of the (F_2) sheath folds and (F_3) synshearing flow folds generated during the regional (D_2) progressive ductile thrusting are presented below.

Synshearing (F_3) flow folds

F_3 folds of the Melness area may be broadly categorized into major and minor structures (e.g. Holdsworth 1990). Major structures include the large-scale transport-parallel antiformal culmination and synformal depressions noted above (Fig. 3a). These open, upright folds lack overturned limbs and can be traced across strike for several kilometres where they may die out or root downwards into underlying ductile thrust mylonite zones (Fig. 3a).

Minor F_3 folds in the Melness area display complex field relationships with both Z and S folds often observed in single exposures. In some cases (e.g. NC 5188 6518), open Z folds are seen to refold earlier S folds (or vice versa), whereas in other situations changes in vergence arise due to the development of curvilinear hinge geometries (e.g. NC 5153 6509). In contrast, many exposures preserve both Z and S folds where no refolding or hinge curvature is apparent and, in these cases, the folds seem to form a conjugate set of asymmetric structures (e.g. NC 5127 6590) (Fig. 4a). In mylonites relatively unaffected by minor folding, centimetre-spaced extensional shear bands are developed, consistently indicating top-to-the-west senses of shear (e.g. NC 5145 6675). Minor F_3 folds are best developed within and adjacent to mylonite zones and define extremely variable orientations ranging from transport-normal to transport-parallel. The dominant type of minor F_3 folds are open–close, gently east-plunging cylindrical structures with hinges trending obliquely or subparallel to the adjacent mineral lineation (Ln) (Fig. 4b). Some, close to isoclinal curvilinear F_3 fold hinges exhibit 90° of curvature and display overall west-directed vergence. Although F_3 folds clearly refold both the mylonitic fabric (Sn) and the east-plunging transport lineation (Ln), they are considered to form part of a kinematicaly linked system of progressive deformation related to continuing west-directed ductile thrusting (Alsop & Holdsworth 2002). There appears to be a change in the dominant sense of minor fold vergence either side of the major culmination trace with Z folds predominating to the south whereas S folds are more common in the region to the north (Fig. 3a). This evidence has in the past been used to suggest that flow perturbations exist on a larger scale, forming structures analogous to surge zones in the more external parts of thrust belts (e.g. Alsop & Holdsworth 1993).

Within the Melness area, S fold hinges are north facing and on average lie about 26° anticlockwise of the mineral lineation (Ln) defining the transport direction. Z folds are south facing and on average lie about 26° clockwise of Ln (Figs 3a,b & 5a,b). Minor F_3 fold hinges measured on the overturned limbs of major F_2 folds typically lie closer to the mineral lineation with mean F_3 Z fold hinges 10° clockwise and mean F_3 S fold hinges 8° anticlockwise of Ln. The strike of the associated fold axial surfaces also displays similar systematic relationships, with mean Z fold axial surfaces around 50° clockwise and mean S fold axial surfaces about 57° anticlockwise with respect to Ln (Figs 3a,e,f,g & 5a,b). The strike of minor F_3 axial planes measured on the overturned limbs of major F_2 folds is typically developed closer to the transport lineation. Thus, both S and Z fold hinges and axial planes display bimodal peaks on distribution graphs (Figs 5a,b & 6a,b) reflecting differing degrees of hinge and axial planar rotation towards ductile thrusts with higher strains concentrated on the overturned limbs of F_2 folds (see Alsop & Holdsworth 2002). Both S and Z F_3 fold hinges and axial planes display broadly similar orientations on either side of the major culmination trace, indicating a lack of subsequent folding or tilting around the major culminations and depressions (Figs 3a–g & 6a,b) (see also discussion of transection and topological relationships between F_2 and F_3 folds). On

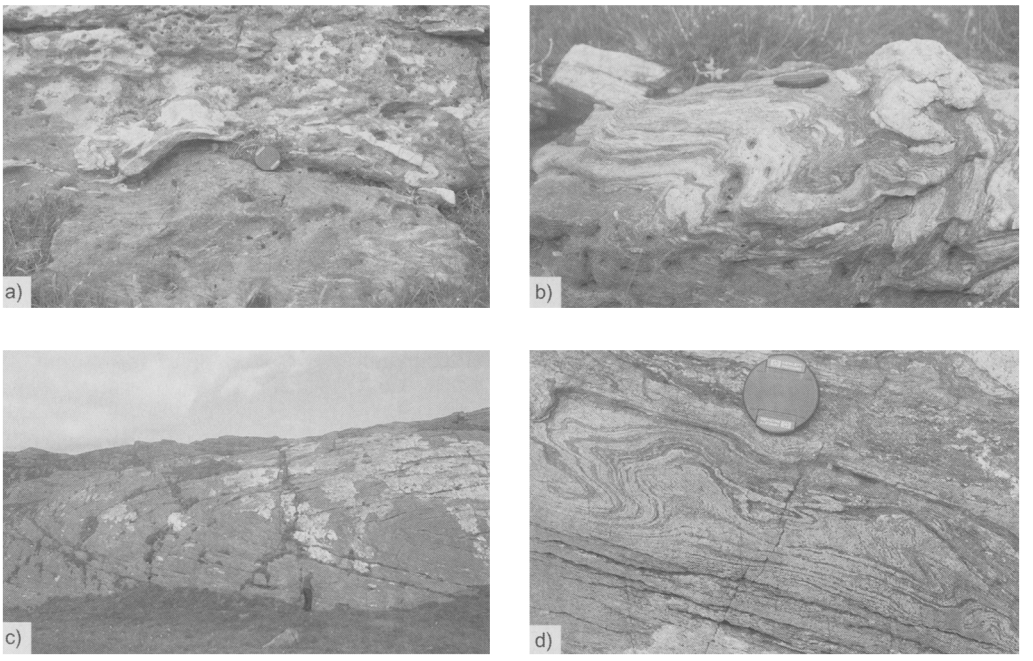

Fig. 4. (**a**) Asymmetric F_3 folds showing a reversal in fold vergence across a minor culmination in mylonites derived from mixed acid–intermediate Lewisianoid gneiss. Photograph looking towards the east down the plunge of F_3 folds on the eastern flank of Cnoc nan Gobhar, Melness. (**b**) Typical minor F_3 asymmetric folds in mylonites derived from mixed acid–intermediate Lewisianoid gneiss. Note traces of refolded F_2 isoclines and folding of mylonitic foliation. Photograph looking towards the east down the plunge of F_3 folds on the eastern flank of Cnoc nan Gobhar, Melness. (**c**) F_2 fold in Moine psammites with more highly attenuated lower (inverted) limb. The hinge of this fold plunges ESE subparallel to the regional mineral lineation (Ln). Photograph looking towards the east on the west flank of Creag Mhor. South of Port Vasgo, Melness. (**d**) Minor F_2 sheath folds in interbanded Moine psammites and semi-pelites showing typical eye-structures and along-strike double vergence patterns. Photograph looking down plunge towards the east on the summit region of Creag Mhor, South of Port Vasgo, Melness.

stereographic projections, mean F_3 S and Z axial planes intersect precisely parallel to the mineral lineation (Ln) (Fig. 3e–g).

In summary, these minor structures appear to be typical of progressive deformation patterns developed during ductile flow in many mylonites (e.g. Evans & White 1984; Ridley 1986). Minor (F_3) synshearing flow folds are mostly gentle to close fold pairs which typically plunge gently east, with associated shallowly east-dipping axial planes. Few curvilinear folds are preserved, with F_3 structures dominated by cylindrical asymmetric S fold hinges and axial planes displaying anticlockwise obliquity to Ln, whereas Z fold hinges and axial planes are clockwise of Ln. All folds are associated with abundant top-to-the-WNW S–C fabrics and shear criteria confirming a progressive system of deformation associated with (D_2) ductile thrusting. The geometry of earlier (F_2) sheath folds, which were generated during the same progressive (D_2) deformation, is now described.

Sheath fold (F_2) structures

Within the Melness area, large-scale transport-parallel antiformal culminations and synformal depressions associated with major F_2 folds almost exactly coincide with the F_3 medial surfaces described above (see Holdsworth 1990; Alsop & Holdsworth 1993, 2002; Alsop *et al.* 1996; Fig. 3a). Minor (F_2) sheath fold hinges are variably distributed over arcs approaching 90° from Ln, with north facing fold hinges consistently developed in a anticlockwise sense to Ln, whereas south facing hinges are clockwise (Fig. 3a,b). The relative structural position of minor folds about the major sheath culmination demonstrates that mean minor folds on the major overturned lower limb (i.e. north-facing Z

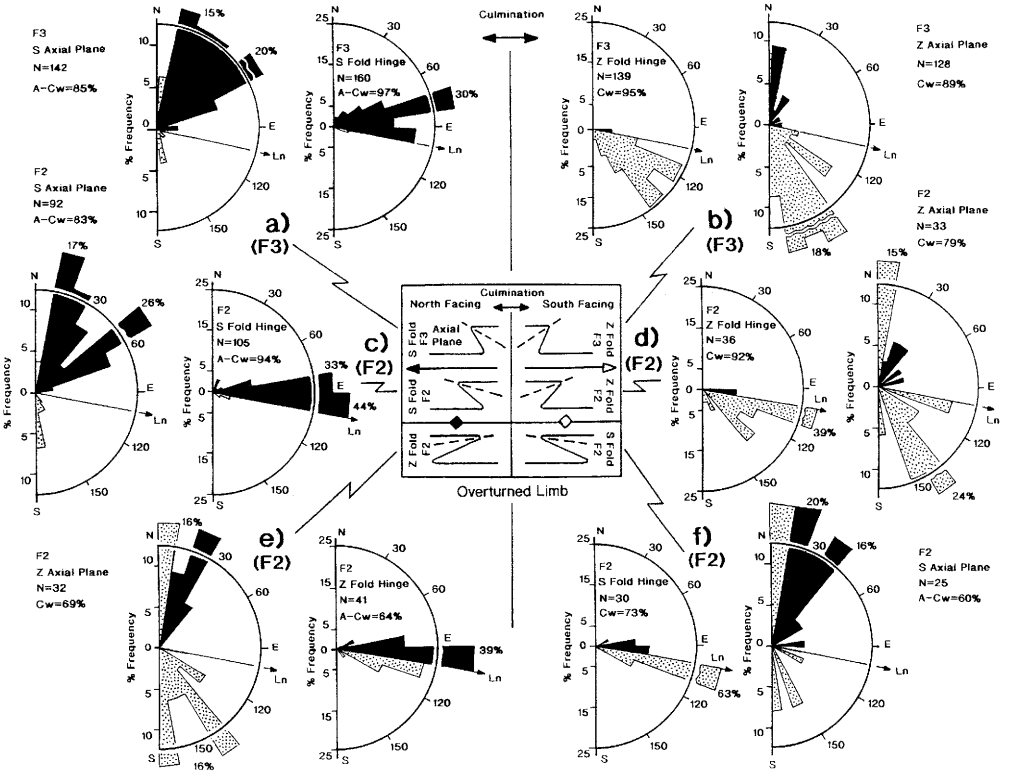

Fig. 5. Detailed structural analysis of folding within the study area illustrating the vergence and obliquity relationships of minor north- and south-facing S and Z folds respectively on either side of the major culmination (refer to Figure 2 for location). The relative obliquity between S and Z fold hinges and associated axial planes with the Ln mineral lineation is shown on rose diagrams for transecting (F_3) flow folds (**a**,**b**), folds forming the upper limbs of (F_2) sheath folds (**c**,**d**) and folds on the overturned lower limbs of sheath folds (**e**,**f**). Fold hinge and axial plane obliquity is measured relative to the adjacent mineral lineation (Ln) and is described as clockwise (Cw) or anticlockwise (A-Cw). F_3 S fold hinges are north facing and on average lie 26° anticlockwise of the mineral lineation (Ln) defining the transport direction. Z folds are south facing and on average lie 26° clockwise of Ln. A consistent overall relationship exists between fold facing and sense of obliquity of minor fold hinges with north-facing hinges being (92%) anticlockwise and south-facing hinges (91%) clockwise of Ln. Associated S axial planes strike (82%) anticlockwise whilst Z axial planes are (84%) clockwise of Ln.

folds and south-facing S folds) plot closest to the mineral lineation (Ln) and have undergone the greatest rotation and deformation (Fig. 5c,d,e,f). A similar pattern is observed on both sides of the major culmination trace demonstrating a lack of pronounced reorientation by the later major synshearing flow folds (Fig. 3a,c,d). Rotations in the strike and dip of minor fold axial planes are governed by the sense of fold asymmetry (S/Z) rather than facing directions. Thus, with increasing deformation on the lower limbs of major sheath folds, mean S fold axial planar strike rotates anticlockwise and mean Z fold axial planes clockwise towards the regional foliation (Sn) marking the shear plane (Figs 3a,e,f,g, 5c,d,e,f & 6c,d,e).

F_2 sheath folds are associated with abundant top-to-the WNW shear criteria generated during (D_2) ductile thrusting. These folds form a series of transport-parallel antiformal culminations and synformal depressions with traces orthogonal to the mylonitic high strain zones. Major F_2 sheath folds with overturned limbs are common, necessitating the use of fold facing directions to discriminate S and Z minor folds on normal or inverted fold limbs (see e.g. Alsop & Holdsworth 1999). Minor (F_2) sheaths are tight to isoclinal folds with mylonitic limbs which on

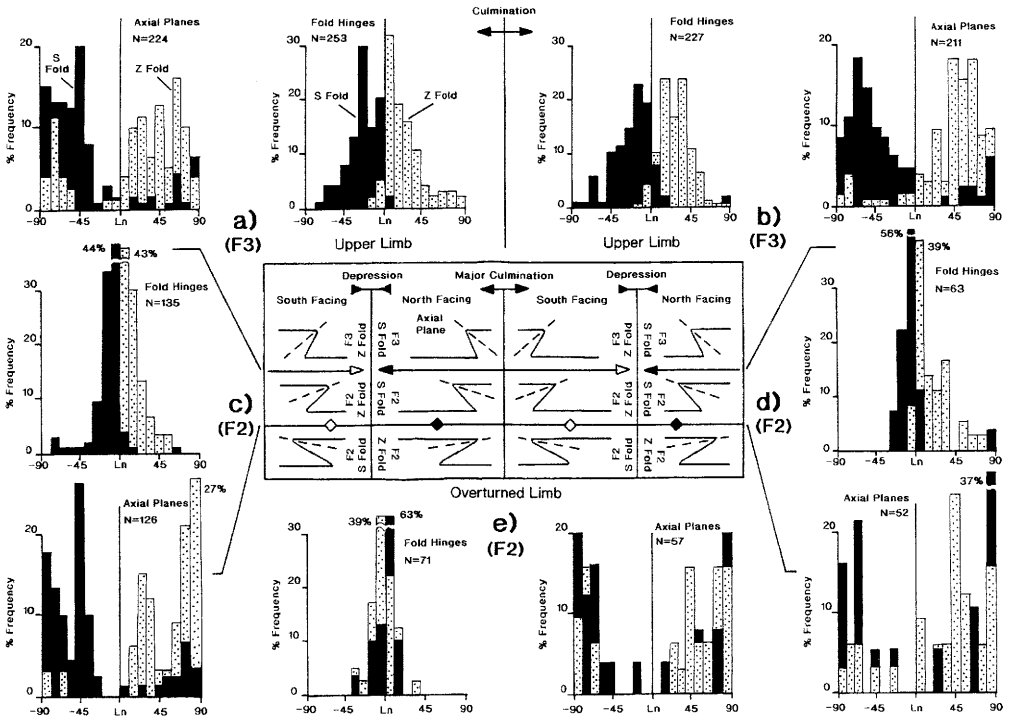

Fig. 6. Frequency distribution histograms of fold hinges and axial planes from the study area orientated relative to the trend of the adjacent Ln transport lineation. The graphs illustrate the vergence and obliquity relationships of minor S folds (solid ornament) and Z folds (stipple ornament) on either side of the major culmination and at varying structural positions around minor medial and axial surfaces (refer to central key for structural position and Fig. 2 for location). The relative obliquity between S and Z fold hinges and associated axial planes with the Ln mineral lineation is shown for transecting (F_3) flow folds (**a**,**b**), folds forming the upper limbs of (F_2) sheath folds (**c**,**d**) and folds on the overturned lower limbs of sheath folds (**e**,**f**). Note the increasing concentration of fold hinges towards Ln and axial planar strikes towards the transport normal from the upper to the lower overturned limbs of sheath folds.

average plunge gently towards the east, with associated shallowly east-dipping axial planes (Fig. 4c). Minor (F_2) curvilinear sheath folds are ubiquitous with north-facing fold hinges anticlockwise of Ln and south-facing fold hinges clockwise of Ln (Fig. 4d). Irrespective of the facing direction, S fold axial planes are typically anticlockwise of Ln and Z fold axial planes clockwise of Ln.

Thus, large-scale (F_2) sheath folds are defined by medial surfaces which coincide in scale, orientation and location with the previously described (F_3) culminations and depressions (Fig. 3a). This correspondence, taken together with the increasingly rotated nature of minor F_3 fold hinges developed on the overturned limbs of F_2 folds, suggests that major F_2 and F_3 structures are closely related in terms of structural mechanisms and controls. Significantly, both minor F_2 and F_3 folds pre-date secondary recrystallization indicating that there are no metamorphic grounds to separate F_2 and F_3 structures (Holdsworth 1987 p. 124). Thus, there is compelling evidence indicating that F_2 and F_3 folds are linked to the same kinematic regime of (D_2) deformation. This paper will now explore the detailed relationships between these fold patterns in order to investigate further the kinematic and geometric evolution of shear zone structures during progressive deformation.

Transection relationships between F_2 sheath folds and F_3 synshearing folds

Geometric investigation of (F_2) sheath folds and adjacent (F_3) synshearing flow folds reveals consistent patterns which display marked structural trends. F_3 flow folds, which obliquely overprint the adjacent F_2 sheath folds may be usefully

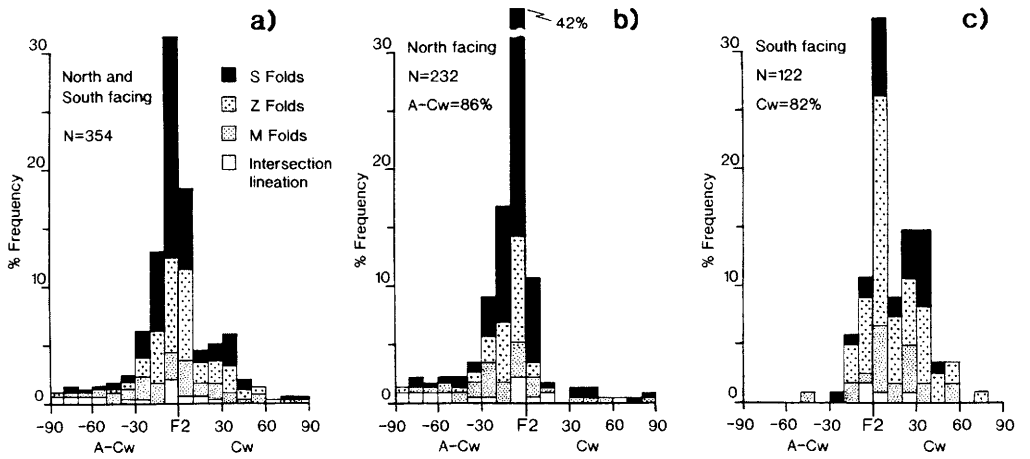

Fig. 7. Frequency distribution histograms of transecting fold hinge angles from the study area orientated either clockwise (Cw) or anticlockwise (A-Cw) relative to the trend of the adjacent F_2 fold hinge. The angle of transection of (F_3) flow folds on sheath folds for all of the study area is given in (**a**), north-facing folds are shown in (**b**), whilst south-facing hinges are displayed in (**c**). North-facing hinges are typically (86%) transected by flow folds in an anticlockwise sense, whereas south-facing sheath folds normally (82%) display clockwise transection.

described in terms of *transecting* (clockwise or anticlockwise) relationships (Fig. 7). An analysis of fold hinge/lineation angles between (F_2) sheath folds and adjacent (F_3) flow folds reveals distinct patterns, with north facing F_2 hinges consistently transected in a anticlockwise (negative) sense by adjacent F_3 hinges, whereas south facing F_2 hinges are transected with a clockwise (positive) obliquity (Fig. 7a–c). Importantly, the sense of transection is independent of fold asymmetry, which is governed by the sense of hinge rotation and hence fold facing. The sense of transection of F_3 synshearing fold hinges and axial surfaces on adjacent minor F_2 sheath folds allows the location of the minor F_2 folds on the major sheath framework to be deduced. Combinations of culmination and depression medial surfaces on antiformal and synformal axial surfaces generate dome and basin (end-member) scenarios in which the eight possible domains are defined uniquely by the sense and combination of fold hinge and axial planar transection (Table 1). Although the sense of fold hinge transection is governed by the direction of F_2 fold rotation (and thereby fold facing), the sense of axial planar transection is controlled by the geometry of the overprinting (Z or S) axial plane (Table 1). This transection grid (Table 1) enables the senses of hinge rotation to be deduced even if no evidence of younging or facing information is preserved. Major basinal sheath fold geometries generate hinge and axial planar transections of the same (synthetic rotations) sense, whilst domal sheaths produce transections of an opposing (antithetic) sense (Table 1).

Topological relationships between F_2 sheath folds and F_3 synshearing folds

Topology may be defined as 'a branch of geometry concerned with those properties of a figure which remain unchanged even when the figure is bent or stretched' (Chambers Dictionary 1993). Fabric topology plots (FTPs) illustrate these invariant or irreversible geometric properties of a body under deformation, and have been used recently to emphasize and monitor planar and linear fabric inter-relationships during progressive shearing (e.g. Alsop & Holdsworth 2002). Importantly, FTPs clearly demonstrate that although *amounts* of angular obliquity between planar and linear fabric elements will vary systematically during deformation, reversals in the *sense* of obliquity will not occur reflecting the inability of planar and linear fabric elements to rotate through the shear plane and shear direction respectively (Ramsay 1980; see Passchier 1997). Consistent and ordered scale-independent relationships between the mineral lineation and fold hinges, fold asymmetries and axial surfaces illustrated on FTPs thus provide a potential record of the generation of folds within mylonites and their subsequent evolution during

Table 1. *Summary transection grid associated with a dome (antiform on culmination) geometry (above) and basin (synform on depression) configuration (below).*

Dome geometry	**Culmination surface**	
	Anticlockwise S hinge obliquity	Clockwise Z hinge obliquity
Upper limb Antithetic transection	**S folds** Anticlockwise transecting hinge Clockwise transecting axial plane	**Z folds** Clockwise transecting hinge Anticlockwise transecting axial plane
Antiformal axial plane		
Lower limb Antithetic transection	**Z folds** Anticlockwise transecting hinge Clockwise transecting axial plane	**S folds** Clockwise transecting hinge Anticlockwise transecting axial plane
Basin geometry	**Depression surface**	
	Clockwise S hinge obliquity	Anticlockwise Z hinge obliquity
Upper limb Synthetic transection	**S folds** Clockwise transecting hinge Clockwise transecting axial plane	**Z folds** Anticlockwise transecting hinge Anticlockwise transecting axial plane
Synformal axial plane		
Lower limb Synthetic transection	**Z folds** Clockwise transecting hinge Clockwise transecting axial plane	**S folds** Anticlockwise transecting hinge Anticlockwise transecting axial plane

Clockwise rotation (relative to Ln trend) will result in the generation of anticlockwise transecting folds and visa versa. The rotation of an axial plane is measured through variations in strike and is governed by the fold vergence, whereas the sense of rotation of fold hinges is dependent on the facing direction and position relative to medial surfaces. Fold hinges may thus be transected with increasing strain in either the same (synthetic) or opposing (antithetic) sense to the associated axial plane depending on structural setting. Each of the eight scenarios around dome and basin geometries are uniquely defined by the combination and sense of fold hinge and axial planar transection of S and Z folds.

continued shearing. The topological relationships between minor (F_3) synshearing folds, and parasitic (F_2) folds developed on the upper and lower (overturned) limbs of major sheath folds are summarized on Fig. 8. The parameters illustrated on this figure are shown for a dip–slip system of deformation but equivalent relationships exist in other kinematic regimes. Fabric topology plots are shown in Fig. 9, and summary FTPs that highlight the relationships between *mean data sets* are shown on Fig. 10 ($n = 750$) and Fig. 11 ($n = 670$).

The angle between the trend of the fold hinge and lineation displays a systematic reduction from transecting F_3 flow folds to the overturned lower limbs of F_2 sheath folds (Fig. 8a). This reflects the increasing rotation of fold hinges towards the shear direction with the greatest deformation on overturned F_2 limbs. Although F_3 hinges are developed closer to Ln on overturned F_2 limbs, the angle they make with minor F_2 hinges is actually larger as the latter are almost colinear with Ln, i.e. minor F_2 hinges undergo a more significant rotation (than F_3) from the upper to lower limbs of major F_2 sheaths. Consequently, the mean angle of F_3 transection increases from the upper to lower limbs of sheath folds (Figs 9a,b & 10a–t; Table 2). The systematic variation in the strike of axial planes about culmination/depression surfaces results in S fold axes (and the associated mineral lineation) typically pitching in a clockwise (positive) sense on NE-trending S axial planes, whilst Z fold hinges (and Ln) pitch in an anticlockwise (negative) sense on SE-striking Z axial planes. Compared to F_2 sheath folds, F_3 hinges display smaller angles of fold hinge pitch on associated axial planes (Figs 8b, 10c,f,m & 11a–t). The angle of hinge pitch transection increases from the upper to lower limbs of sheath folds reflecting greater F_2 hinge rotation on lower limbs (Table 2). As the angle (and sense) of lineation pitch is also measured from the strike of the (Z or S) axial plane, it therefore increases from F_3 flow folds to the lower limbs of sheath folds (Figs 8c, 10d,n & 11d,n). The angle of lineation pitch transection similarly increases from the upper to lower limbs of sheath folds (Table 2). Increasing rotation of fold hinges towards the shear direction with greater

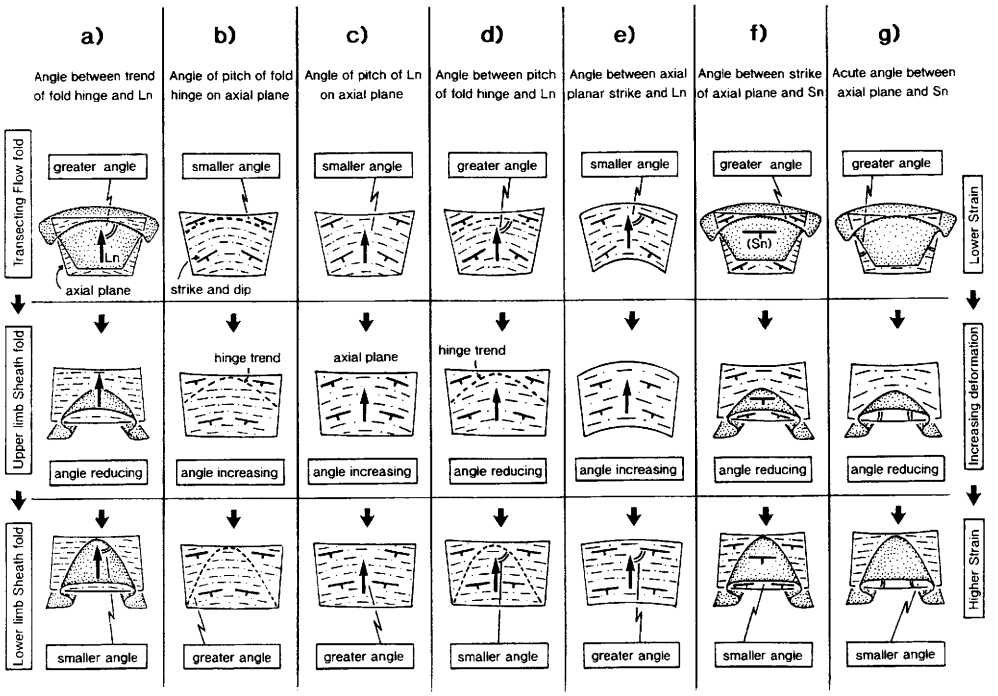

Fig. 8. Schematic sketches illustrating the geometric consequences of fold and fabric rotations associated with increasing deformation from transecting (F_3) flow folds (upper row) to the lower limbs of (F_2) sheath folds (lower row). Lower strain situations for each parameter (**a**–**g**) are thus given in the upper row, whilst the higher strain situation for each relationship are shown below. Angular relationships between parameters may increase or decrease with increasing deformation, and are frequently related to the orientation of foliation (Sn) and the transport-parallel lineation (Ln).

deformation results in a systematic reduction in the angle between the pitch of a fold hinge and adjacent lineation from F_3 folds to the overturned lower limbs of sheath folds (Fig. 8d). The mean angle of F_3 transection thus increases from the upper to lower limbs of sheath folds (Figs 10e,g,q & 11e,g,q; Table 2). The angle between the strike of the axial plane and the trend of the adjacent lineation displays a systematic increase from F_3 folds to the overturned lower limbs of sheath folds (Fig. 8e). This reflects the increasing rotation of axial planes towards the shear plane with greater deformation. The mean angle of F_3 axial planar transection therefore increases from the upper to lower limbs of sheath folds (Figs 10h,r & 11h,r; Table 2). Increasing rotation of axial planes towards the foliation (shear) plane results in a systematic reduction in the angle between axial planar strike and the trend of the adjacent foliation from F_3 flow folds to the lower limbs of sheath folds (Fig. 8f). Consequently, the mean angle of F_3 axial planar transection increases from the upper to lower limbs of sheath folds (Figs 10i,s, 11a–j, s; Table 2). Similarly, the acute angle between the axial plane and the adjacent foliation displays a systematic reduction from F_3 folds to the overturned lower limbs of sheath folds, whereas the mean angle of F_3 axial planar transection shows a concomitant increase (Figs 8g, 10j,t & 11j,t; Table 2).

In summary, both F_2 and F_3 folds are associated with top-to-the-WNW thrusting, although their age relative to the local (Sn) fabric differs with F_2 folds displaying mylonitic limbs and F_3 structures refold this foliation. Minor fold hinges display sequential rotations towards the transport direction with the angle of obliquity systematically reducing from (F_3) synshearing flow folds to the upper limbs of (F_2) sheath folds to the higher strained and overturned lower limbs. Minor fold axial planes display concomitant rotations towards the foliation plane. Thus, fold hinge and axial plane transection angles increase from the upper to lower limbs of sheath folds reflecting the greater deformation and fabric rotation on the lower sheath limbs

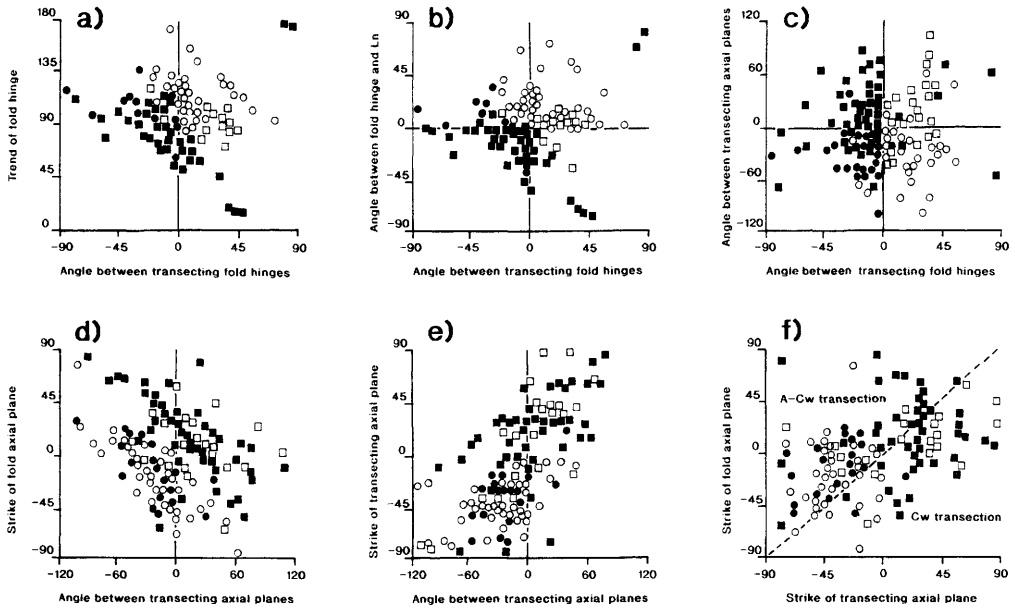

Figure 9. Fabric topology plots of sheath fold and flow fold data from the study area. South-facing data is shown by open symbols and north-facing data is shown by solid symbols. In each case, structures associated with Z (circles), or S (squares) (F_2) sheath folds are shown with positive clockwise (Cw) or negative anticlockwise (A-Cw) trends relative to adjacent transecting (F_3) flow folds. Fold trend values are given between 0° and 180°, but values of axial planar strike are displayed for 90° either side of 0° strike, to show the continuation of geometric trends across the north–south direction. The upper row of plots shows how the angle of (F_2) sheath fold hinge transection by (F_3) flow folds varies in relation to (**a**) trend of sheath fold hinges, (**b**) angle between sheath fold hinge and adjacent mineral lineation (Ln), (**c**) angle between adjacent transecting axial planes. The lower row of plots shows how the angle of axial planar transection between sheath folds and flow folds varies in relation to (**d**) strike of sheath fold axial planes, (**e**) strike of flow fold axial planes. A comparison of sheath and flow fold axial planar strikes and resultant angles of clockwise (Cw) and anticlockwise (A-Cw) transection is given in (**f**).

(Table 2). These geometric relationships are now discussed in terms of alternative models for overall fold and fabric evolution within a system of progressive (D_2) deformation.

Discussion of curvilinear fold patterns and evolution

General observations and inferences of progressive deformation forming successive generations of curvilinear folds have been made at a variety of scales from outcrop (e.g. Ghosh & Sengupta 1984, 1987; Ghosh *et al.* 1999) to regional (e.g. Goscombe 1991; Alsop 1994). The detailed analyses of synshearing and sheath folds presented in this study is based on fabric development across both axial surfaces and medial (culmination/depression) surfaces reflecting the 3D nature of such deformation systems. Such an examination also enables the progressive structural development to be assessed. A variety of alternative models for the development of synshearing folds and their relationships to earlier sheath folds are now discussed.

Fold evolution model

The fold evolution model suggests that the orientation and asymmetry of synshearing (F_3) folds is directly controlled by variable displacement along underlying detachments. The orientation and asymmetry of the folding is a direct consequence and product of perturbations in ductile flow which are both transient and scale independent (Holdsworth 1990; Alsop & Holdsworth 1993, 2002). In this model, differential dextral and sinistral shear will generate S and Z folds with consistent anticlockwise and clockwise obliquities to Ln respectively (Fig. 1c). Such folds may then subsequently undergo a degree of hinge rotation towards the transport

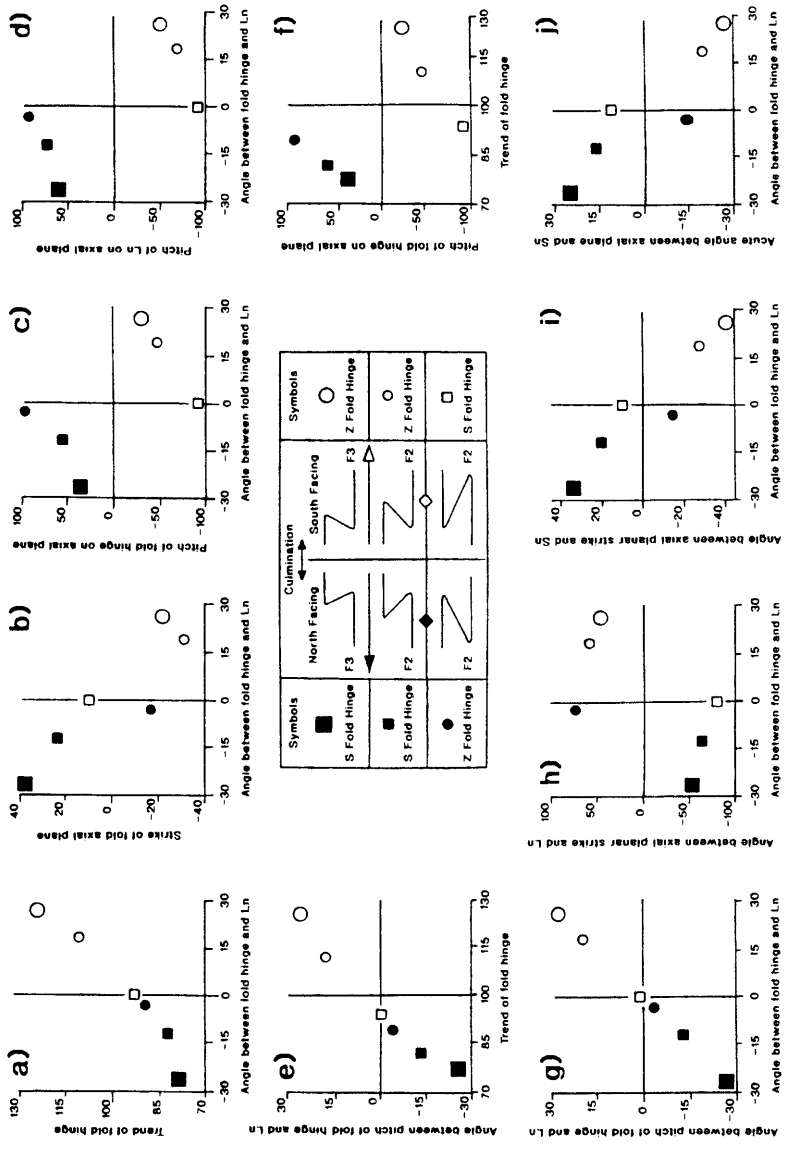
a)
Trend of fold hinge
Angle between fold hinge and Ln
b)
Strike of fold axial plane
Angle between fold hinge and Ln
c)
Pitch of fold hinge on axial plane
Angle between fold hinge and Ln
d)
Pitch of Ln on axial plane
Angle between fold hinge and Ln
e)
Angle between pitch of fold hinge and Ln
Trend of fold hinge
f)
Pitch of fold hinge on axial plane
Trend of fold hinge
Culmination
North Facing
South Facing
Symbols
S Fold Hinge
Z Fold Hinge
F3
F2
g)
Angle between pitch of fold hinge and Ln
Angle between fold hinge and Ln
h)
Angle between axial planar strike and Ln
Angle between fold hinge and Ln
i)
Angle between axial planar strike and Sn
Angle between fold hinge and Ln
j)
Acute angle between axial plane and Sn
Angle between fold hinge and Ln

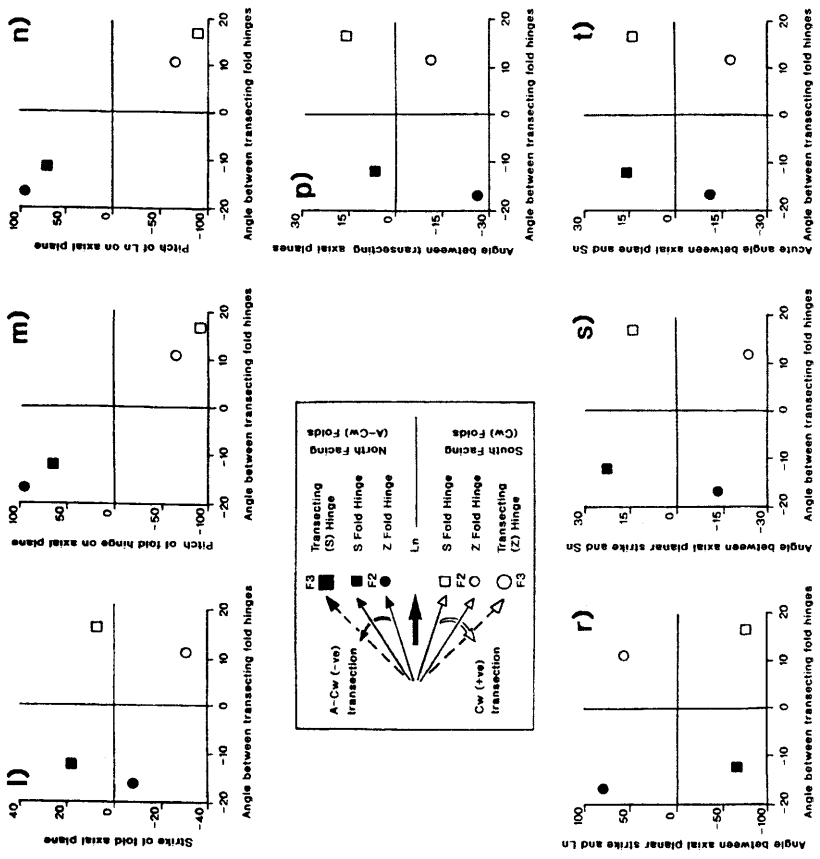

Fig. 10. Summary fabric topology plots showing the mean orientation ($n = 750$) of Z (circles) and S (squares) fold hinge trends relative to the trend of the adjacent lineation (Ln) (**a–j**). In each case, north-facing folds are shown by the solid symbols; south-facing structures are given by the open symbols. Note how north-facing fold hinges are anticlockwise of Ln and south-facing folds are clockwise. A guide to symbols and structural position is given in the central transport-normal section/key with transecting (F_3) flow folds shown on the upper row (larger symbols). The relative location of the culmination surface and the antiformal axial plane results in the range of minor fold geometries depicted. The lower set of FTPs (**k–t**) show the angle of transection of mean (F_2) sheath fold hinge trends by adjacent (F_3) flow fold hinges. Note that north-facing fold hinges are consistently transected in a (negative) anticlockwise sense and south-facing hinges in a (positive) clockwise sense (see central plan for obliquities and symbols). The various structural parameters display systematic and sequential variations from F_3 flow folds, to the upper limbs of F_2 sheath folds to lower limbs of sheath folds.

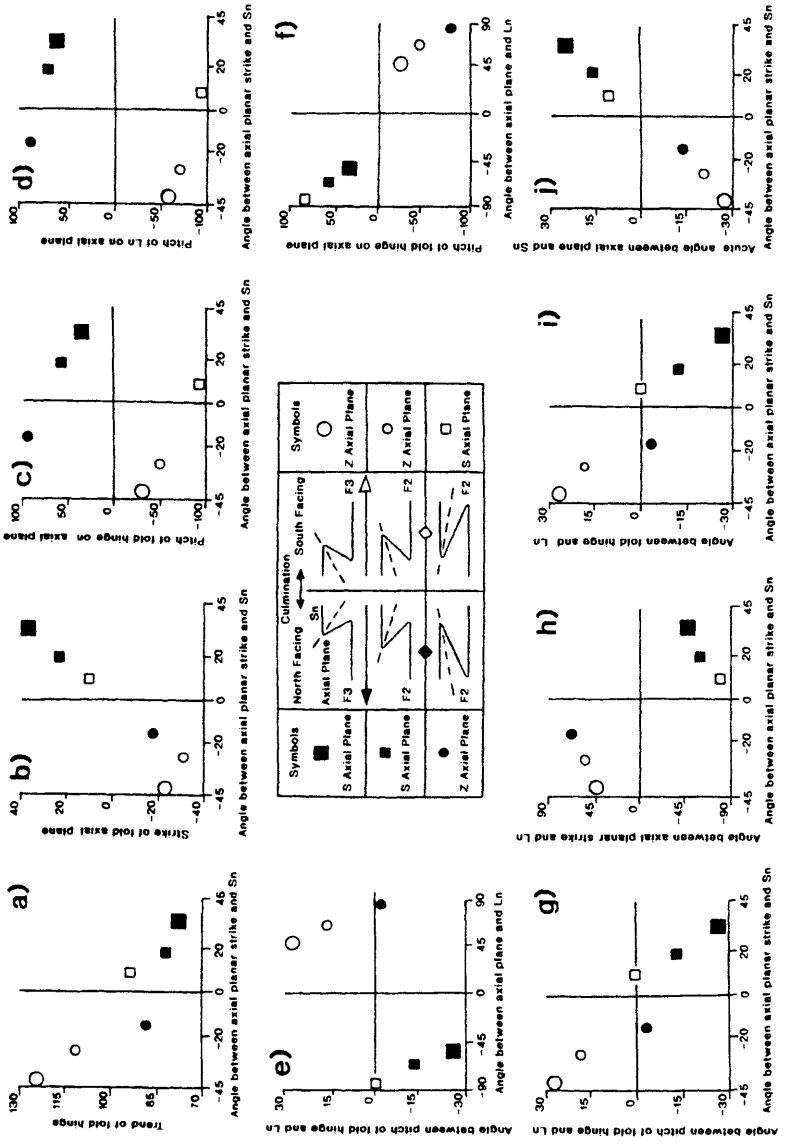
a)
Trend of fold hinge
Angle between axial planar strike and Sn
b)
Strike of fold axial plane
Angle between axial planar strike and Sn
c)
Pitch of fold hinge on axial plane
Angle between axial planar strike and Sn
d)
Pitch of Ln on axial plane
Angle between axial planar strike and Sn
e)
Angle between pitch of fold hinge and Ln
Angle between axial plane and Ln
f)
Pitch of fold hinge on axial plane
Angle between axial plane and Ln
g)
Angle between pitch of fold hinge and Ln
Angle between axial planar strike and Sn
h)
Angle between axial planar strike and Ln
Angle between axial planar strike and Sn
i)
Angle between fold hinge and Ln
Angle between axial planar strike and Sn
j)
Acute angle between axial plane and Sn
Angle between axial planar strike and Sn
Symbols
North Facing
Culmination
South Facing
Symbols
Axial Plane
Sn
F3
F2
Z Axial Plane
S Axial Plane

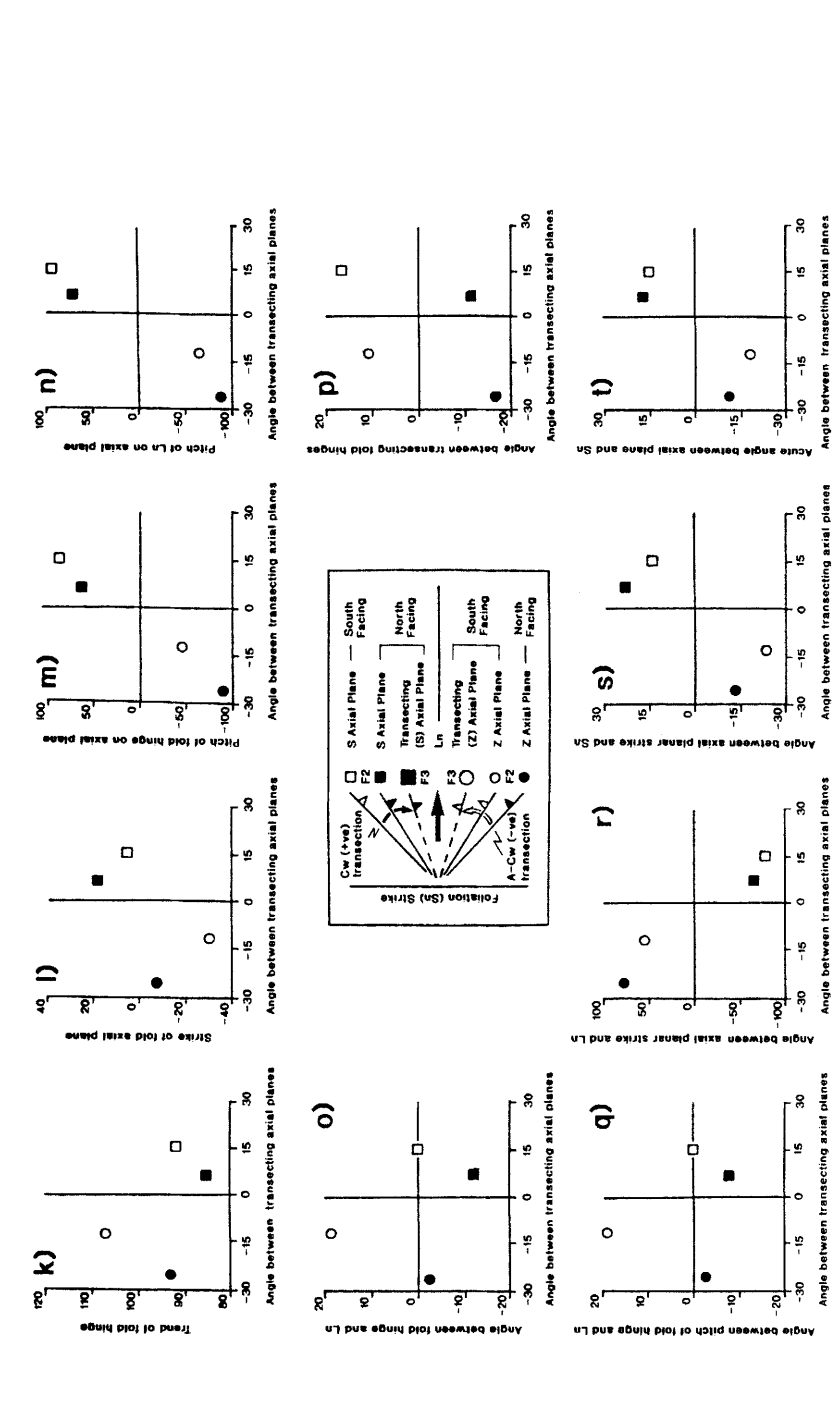

Fig. 11. Summary fabric topology plots showing the mean orientation ($n = 670$) of Z (circles) and S (squares) fold axial planar strikes relative to the trend of the adjacent foliation (Sn) (**a**–**j**) and lineation (Ln) (**e**,**f**). In each case, north-facing folds are shown by the solid symbols; south-facing structures are given by the open symbols. Note how Z and S fold axial planes are consistently anticlockwise (negative) and clockwise of the mean Sn trend. A guide to symbols and structural position is given in the central transport-normal section/ key with transecting flow folds shown on the upper row (larger symbols). The relative location of the culmination surface and the antiformal axial plane results in the range of minor fold geometries depicted. The lower set of FTP's (**k**–**t**) show the angle of transection of (F_2) sheath fold axial planar strike by adjacent (F_3) flow fold axial planes. Note that S axial planes are consistently transected in a positive clockwise sense and Z axial planes in a (negative) anticlockwise sense (see central plan for obliquities and symbols). The various structural parameters display systematic variations from flow folds, to the upper and lower limbs of sheath folds.

Table 2. *Summary table of angular obliquities associated with a–g structural parameters in the study area.*

	North facing		Culmination surface		South facing	
Structural parameter	Upper limb trans.	**Difference in trans. across axial surface**	Lower limb trans.	Lower limb trans.	**Difference in trans. across axial surface**	Upper limb trans.
a)	–14°	**–9°**	–23°	+22°	**+18°**	+3°
b)	+18°	**+38°**	+56°	–64°	**–50°**	–14°
c)	+9°	**+20°**	+29°	–39°	**–27°**	–12°
d)	–9°	**–19°**	–28°	+26°	**+23°**	+3°
e)	–3°	**+17°**	+14°	–9°	**–9°**	0°
f)	+20°	**–52°**	–32°	+29°	**+53°**	–24°
g)	19°	**+3°**	22°	22°	**+4°**	18°

The table summarizes mean F_3 transection (Trans.) data across the axial surface of major F_2 folds (upper and lower limbs), on both the north-facing (left) and south-facing (right) margins of the major culmination. In each case, data refers to the sense and amount of mean angular transection and indicates that lower (F_2) fold limbs have undergone greater rotation and hence larger angles of transection. Structural parameters: **a)** Angle between trend of fold hinge and lineation; **b)** Angle of fold hinge pitch on axial plane; **c)** Angle of lineation pitch on axial plane; **d)** Angle between pitch of fold hinge and lineation; **e)** Angle between axial planar strike and lineation trend; **f)** Angle between axial planar strike and trend of foliation; **g)** Acute angle between axial plane and long-limb foliation. Refer to Fig. 8 and text for further details.

direction raising the question as to whether sheath folds could initiate by a similar process (Fig. 1d). In such a model F_2 sheath folds simply represent early flow perturbation folds subsequently modified by high-strain shearing. Although the common evolutionary patterns on many fabric topology plots from F_3 synshearing folds to F_2 sheath folds may be taken to support such an interpretation, a number of important differences exist.

The general lack of F_3 sheath folds might suggest that a different process is responsible for creating the earlier (F_2) sheath folds. Importantly, F_2 sheath folds describe a complete arc of hinge orientations from transport-normal to transport-parallel, with some hinges still preserved at high angles to transport (Fig. 1b; Holdsworth 1988; Alsop & Holdsworth 1999). F_3 folds do not describe such a pronounced arc and typically initiate at smaller (oblique) angles to transport than sheath folds (Fig. 1a,c). They also lack pronounced overturned limbs (see Alsop & Holdsworth 2002). If sheaths were initiated by flow perturbations, this suggests that the geometry of the flow cell was different from those that created the F_3 folds. Thus, although F_2 and F_3 folds clearly belong to a progressive (D_2) deformation, the angles of F_2 and F_3 fold initiation appear to be quite different. This may require an alternative model for generating geometrically distinct but related fold phases to be considered.

Fold inheritance model

The fold inheritance model suggests that the orientation and asymmetry of synshearing (F_3) folds is directly controlled by the pre-existing attitude of layering. The orientation of the mean regional foliation (Sn) and lineation (Ln) displays limited but recognizable variation to the north and south of the major transport-parallel culmination trace which bisects the Melness study area (Figs 3b–d & 12). This variation in fabric attitudes is simply a consequence of reverse asymmetry vergence where the long limbs of minor folds (with opposing vergence) remain subparallel to one another across the medial surface (Fig. 13; see also fig. 9 Alsop & Holdsworth 2002). Clearly, this differs from normal asymmetry vergence patterns where the long limbs of minor folds are rotated normally resulting in markedly different attitudes on either side of a major fold and the classical stereographic girdle pattern.

The variations in the mean statistical orientation of the layering (Sn) about the major (F_2) culminations may however be significant in relation to F_3 fold development as layering which is oblique to the axes of the bulk strain ellipsoid will generate fold hinges that initiate perpendicular to the direction of shortening *within* that layer (Flinn 1962; Treagus & Treagus 1981). The orientation and geometry of such fold hinges, which consistently form parallel to the long axis of the sectional ellipse within the

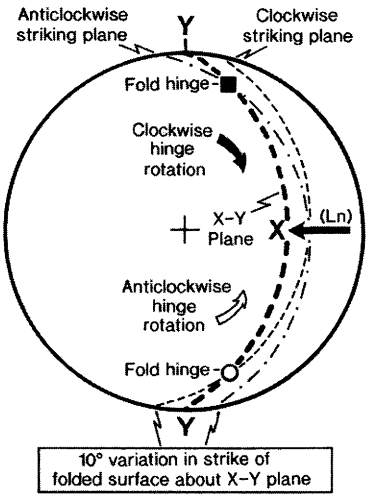

Mean Melness data	X-Yplane (S2)	Folded surface(Sn)	X	Y	X-Y/Sn intersection	Intersection obliquity
North Culmination	176/29E	172/23E	096	6/005	9/007	2°Cw (fromY) 88°ACw (fromX)
South Culmination	178/24E	001/22E	097	4/008	11/151	39°ACw (fromY) 51°Cw (fromX)

Fig. 12. Schematic stereographic plot illustrating how layering developed oblique to the *X*, *Y*, *Z* axes of the finite strain ellipsoid will develop folds of differing orientations (see Treagus & Treagus 1981). In this example, layering which strikes anticlockwise of the *X*–*Y* plane will initiate folding anticlockwise of transport (*X*), whilst layering which strikes clockwise of the *X*–*Y* plane will initiate folding clockwise of transport. The sense of subsequent fold hinge rotation during progressive deformation is also shown whereas the table shows the calculated mean data for either side of the major culmination in the Melness case study area. Different mean orientations of the folded surface (Sn) to the north and south of the culmination will encourage folds to initiate with an opposing sense of obliquity to Ln (*X*).

layer, will thus be governed by and vary according to, the relative obliquities between layering and the strain ellipse, together with subsequent rotations associated with angular migration of the fold axis during progressive deformation (Treagus & Treagus 1981; Carreras 1997) (Fig. 12). A reversal in the sense of obliquity of layering to the strain ellipsoid will generate a reversal in apparent differential shear as the layer rotates towards the *X*–*Y* plane. Thus, systematic variations in the orientation of layering relative to the bulk strain ellipsoid will result in folds initiating with reversed senses of clockwise or anticlockwise obliquity to the *X* direction. These will subsequently undergo opposing senses of hinge rotation during progressive shear. To the north of the major culmination, mean Sn layering intersects the mean S_2 fabric representing the *X*–*Y* plane of the strain ellipsoid in a clockwise sense (relative to the intermediate *Y* axis), whereas to the south of the culmination the equivalent intersection is anticlockwise of *Y* (Fig. 12).

In summary, antiformal culminations and synformal depressions associated with F_2 sheath folding may impart a consistent obliquity between the bulk strain ellipse and layering, which will reverse on opposing flanks of culminations and depressions. This inherited architecture will also govern the orientation of subsequent F_3 fold hinges and thereby control the sense of F_2–F_3 transection and direction of F_3 hinge rotations. Thus, geometric patterns developed during F_2 sheath folding could control subsequent F_3 medial surfaces resulting in the observed coincidence of F_2 and F_3 culmination and depression surfaces (Fig. 13).

Within the geometric model outlined above, the orientation and asymmetry of F_3 synshearing folds is entirely controlled by the pre-existing attitude of the layering following F_2 folding. A significant issue raised by this model is our inability to define the attitude of this post-F_2 layering precisely. These post-F_2 orientations are critical to the integrity of the fold inheritance model, but remain largely unresolved owing to the overprinting F_3 deformation. In addition, layering may change orientation from the upper to lower overturned limbs of F_2 folds, thereby also generating a reversal in subsequent F_3 vergence and orientation. However, the ability to trace consistent F_3 vergence across F_2 axial surfaces suggests that such a switch in asymmetry does not generally develop. This may arguably reflect increasing D_2 strain on overturned (F_2) limbs which negates any significant obliquity in layering orientation (Fig. 13). Alternatively, this relationship may suggest that the overall coincidence of F_2 and F_3 patterns is not entirely explained by superposition of F_3 on F_2 structures in the fold inheritance fold model.

Hybrid fold model

The hybrid fold model suggests that the orientation and asymmetry of synshearing (F_3) folds is directly controlled by variable components of both the fold evolution and inheritance models. Regions lacking pronounced F_2 sheath folding do not develop transport parallel F_3 culminations and depressions (Alsop & Holdsworth 1993). In contrast, the Melness area is marked by a major F_2 sheath culmination which coincides with transport-parallel F_3 folding. Such

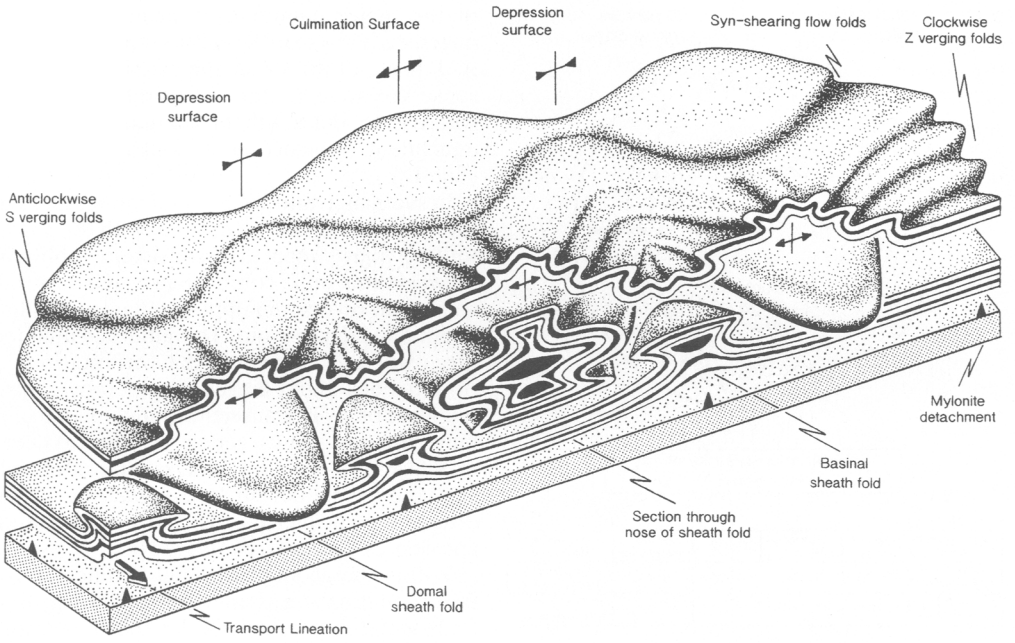

Fig. 13. Schematic 3D cartoon illustrating the geometry and orientation of synshearing flow folds together with sheath folds associated with transport-parallel culmination and depression surfaces. Increasing deformation towards the underlying detachment surface (marked by barbs) results in pronounced attenuation of the lower fold limb and reduction in the apical angle of the sheath fold from tongue folds on the upper limb to tubular folds on the lower limb. Culmination and depression surfaces are associated with transport-parallel neutral verging (M) open folds with steeply dipping axial planes. They separate regions of synshearing flow folds with S folds trending anticlockwise of transport from Z folds developed clockwise of transport.

variations have in the past been attributed to the different geometries of flow perturbation cells (e.g. Alsop & Holdsworth 1993; Alsop *et al.* 1996). However, they may also be interpreted in terms of F_2 folds exerting a clear control on the geometry of subsequent F_3 folds at least on a larger kilometric scale. Within such a scenario, pre-existing F_2 sheaths may exert a geometric influence on F_3 folds (*fold inheritance model*) whilst at the same time constraining the location and scale of subsequent flow perturbation cells (*fold evolution model*). Hybrid fold models incorporating flow perturbations and a component of inherited geometric constraint (perhaps concentrated in the lower-strain regions of earlier F_2 folds) may thus also be applicable.

Conclusions

These natural fold patterns systematically record and reflect the kinematics and evolution of flow within shear zones. However the inevitable overprinting of structures that occurs during progressive deformation means that the interpretation of the preserved relationships is somewhat ambiguous. Fabric topology plots (FTPs) are of value in such situations as they clearly and effectively monitor fold and fabric relationships during progressive deformation. These plots demonstrate that synshearing F_3 flow folds and F_2 sheath folds share many geometric properties and display a common evolutionary sequence from larger through to smaller obliquities respectively (Fig. 13). FTPs can be used to highlight geometric patterns of structural evolution in which fabric relationships may undergo modification (but not reversal) during kinematically coherent flow.

Synshearing F_3 folds display a consistent sense of either clockwise (Z fold) or anticlockwise (S fold) hinge transection on the earlier F_2 sheath folds. The *sense* of transection (which is governed by the direction of hinge rotation) switches across the medial (culmination/depression) surface and thus acts as a reliable indicator of clockwise or anticlockwise rotation. The sense of transection will therefore predict the

polarity of fold facing even in areas lacking stratigraphic control and/or abundant evidence of younging. The *amount* of transection increases from the upper to lower limbs of sheath folds, reflecting larger fabric rotations associated with greater deformation on the overturned (lower) limb setting (Fig. 13). Similar, predictable patterns may occur in all situations where folds are associated with shear zones. The sense of axial planar transection is governed by the asymmetry of (Z or S) folding and therefore reverses across both medial surfaces and axial surfaces. F_2 Z axial planar strike is transected (by F_3) in an anticlockwise sense (reflecting a clockwise F_2 rotation) whereas S fold axial planes are transected (by F_3) in a clockwise sense. Thus, the sense of axial planar transection is governed by fold (Z or S) asymmetry, and the sense of hinge transection is controlled by the direction of hinge rotation and thereby the polarity of fold facing. Combining hinge and axial plane transection relationships on a *transection grid* allows the position of minor F_2 folds to be uniquely located on major F_2 sheath folds.

Foliation-normal and transport-parallel culmination and depression surfaces generated during F_2 and F_3 folding correspond with one another in terms of scale, space and orientation reflecting common origins and generation during progressive (D_2) shearing (Fig. 13). The concurrence of culminations and depressions defined by the (F_2) sheath folds and synshearing (F_3) folds is particularly important with regard to an overall understanding of the progressive (D_2) deformation. This coincidental relationship is interpreted in the fold evolution model to suggest that the sheath folds are genetically and kinematically related to flow perturbation cells, similar to those proposed previously to explain the distribution and geometry of the F_3 folds in Melness and other areas. However, F_3 'eye-shaped' closures and obvious curvilinear folds are scarce, with F_3 folds notably exhibiting different angles of hinge initiation compared to F_2 sheath folds. Alternatively, the fold inheritance model suggests that development of the earlier (F_2) sheath folds may influence and pre-determine the geometry and distribution of later synshearing (F_3) flow folds. Although it is difficult to define the orientation of post-F_2 layering, it may be expected to display differing attitudes across the axial surfaces of major F_2 folds, and hence generate a reversal in F_3 fold vergence. However, our detailed observations suggest the contrary with F_3 folds maintaining constant asymmetry across the (F_2) axial surfaces. A combination of these two models, as suggested in the hybrid fold model, is also entirely feasible and perhaps most applicable in regions where major early fold systems arch mylonitic fabrics and foliations in which the synshearing folds will subsequently develop. Clearly such systems may become extremely complex and to some extent self sustaining as the geometric influence of successive fold sets systematically influences the nature and kinematics of subsequent deformation.

Fieldwork for this paper was funded under the NERC-BGS-Academic mapping programme awarded to the University of Durham (Grant F60/G2/36). Subsequent additional funding was provided from the Edinburgh Geological Society and the Welch bequest of the University of St Andrews. Jordi Carreras and Graham Potts provided careful and constructive reviews.

References

ALSOP, G.I. 1992. Progressive deformation and the rotation of contemporary fold axes in the Ballybofey Nappe, northwest Ireland. *Geological Journal*, **27**, 271–283.

ALSOP, G.I. 1994. Relationships between distributed and localized shear in the tectonic evolution of a Caledonian fold and thrust zone, northwest Ireland. *Geological Magazine*, **131**, 123–136.

ALSOP, G.I. & HOLDSWORTH, R.E. 1993. The distribution, geometry and kinematic significance of Caledonian buckle folds in the western Moine Nappe, northwestern Scotland. *Geological Magazine*, **130**, 353–362.

ALSOP, G.I. & HOLDSWORTH, R.E. 1999. Vergence and facing patterns in large-scale sheath folds. *Journal of Structural Geology*, **21**, 1335–1349.

ALSOP, G.I. & HOLDSWORTH, R.E. 2002. The geometry and kinematics of flow perturbation folds. *Tectonophysics*, **350**, 99–125.

ALSOP, G.I., HOLDSWORTH, R.E. & STRACHAN, R.A. 1996. Transport-parallel cross folds within a mid-crustal Caledonian thrust stack, northern Scotland. *Journal of Structural Geology*, **18**, 783–790.

BELL, T.H. 1978. Progressive deformation and reorientation of fold axes in a ductile mylonite zone: the Woodroffe thrust. *Tectonophysics*, **44**, 285–321.

BERTHÉ, D. & BRUN, J.P. 1980. Evolution of folds during progressive shear in the South Amorican Shear Zone, France. *Journal of Structural Geology*, **2**, 127–133.

BOLHAR, R. & RING, U. 2001. Deformation history of the Yola Bolly terrane at Leech Lake Mountain, Eastern belt, Franciscan subduction complex, California Coast ranges. *Geological Society of America Bulletin*, **113**, 181–195.

BRITISH GEOLOGICAL SURVEY 1997. Tongue, Scotland 114E. Solid Geology. 1:50,000.

BRITISH GEOLOGICAL SURVEY 2002. Loch Eriboll, Scotland 114W. Solid Geology. 1:50,000.

BRYANT, B. & REED, J.C. 1969. Significance of lineation and minor folds near major thrust faults in the southern Appalachians and the British and Norwegian Caledonides. *Geological Magazine*, **106**, 412–429.

CARRERAS, J. 1997. Shear zones in foliated rocks: geometry and kinematics. *In*: SENGUPTA, S. (ed.) *Evolution of geological structures in micro- to macro-scales*, pp. 185–201. Chapman & Hall, London.

CARRERAS, J., ESTRADA, A. & WHITE, S. 1977. The effect of folding on the c-axis fabrics of a quartz mylonite. *Tectonophysics*, **39**, 3–24.

CHAMBERS DICTIONARY 1993. Chambers Harrap Publishers Ltd. Edinburgh. 2062 pp.

COBBOLD, P.R. & QUINQUIS, H. 1980. Development of sheath folds in shear regimes. *Journal of Structural Geology*, **2**, 119–126.

CONEY, P.J. 1974. Structural analysis of the Snake Range 'Decollement', East-Central Nevada. *Geological Society of America Bulletin*, **85**, 973–978.

COWARD, M.P. & POTTS, G.J. 1983. Complex strain patterns developed at the frontal and lateral tips to shear zones and thrust zones. *Journal of Structural Geology*, **5**, 383–399.

DILLON, J.T., HAXEL, G.B. & TOSDAL, R.M. 1990. Structural evidence for northeastward movement on the Chocolate Mountains Thrust, southeasternmost California. *Journal of Geophysical Research*, **95**, 19953–19971.

ESCHER, A. & WATTERSON, J. 1974. Stretching fabrics, folds and crustal shortening. *Tectonophysics*, **22**, 223–231.

EVANS, D.J. & WHITE, S.H. 1984. Microstructural and fabric studies from the rocks of the Moine Nappe, Eriboll, NW Scotland. *Journal of Structural Geology*, **6**, 369–389.

EZ, V. 2000. When shearing is a cause of folding. *Earth Science Reviews*, **51**, 155–172.

FLETCHER, J.M. & BARTLEY, J.M. 1994. Constrictional strain in a non-coaxial shear zone: implications for fold and rock fabric development, central Mojave metamorphic core complex, California. *Journal of Structural Geology*, **16**, 555–570.

FLINN, D. 1962. On folding during three-dimensional progressive deformation. *Quarterly Journal of the Geological Society of London*, **118**, 385–433.

FOSSEN, H. & RYKKELID, E. 1990. Shear zone structures in the Øygarden area, West Norway. *Tectonophysics*, **174**, 385–397.

GHOSH, S.K. & SENGUPTA, S. 1984. Successive development of plane noncylindrical folds in progressive deformation. *Journal of Structural Geology*, **6**, 703–709.

GHOSH, S.K. & SENGUPTA, S. 1987. Progressive development of structures in a ductile shear zone. *Journal of Structural Geology*, **9**, 277–287.

GHOSH, S.K., HAZRA, S. & SENGUPTA, S. 1999. Planar, non-planar and refolded sheath folds in the Phulad Shear Zone, Rajasthan, India. *Journal of Structural Geology*, **21**, 1715–1729.

GOSCOMBE, B. 1991. Intense non-coaxial shear and the development of mega-scale sheath folds in the Arunta Block, Central Australia. *Journal of Structural Geology*, **13**, 299–318.

HANSEN, E. 1971. *Strain Facies*. New York, Springer-Verlag.

HENDERSON, J.R. 1981. Structural analysis of sheath folds with horizontal X-axes, northeast Canada. *Journal of Structural Geology*, **3**, 203–210.

HARRIS, L.B., KOYI, H.A. & FOSSEN, H. 2002. Mechanisms of folding of high-grade rocks in extensional tectonic settings. *Earth Science Reviews*, **59**, 163–210.

HOBBS, B.E., MEANS, W.D. & WILLIAMS, P.F. 1976. *An outline of structural geology*. John Wiley & Sons, New York.

HOLDSWORTH, R.E. 1987. Basement/cover relationships, reworking and Caledonian ductile thrust tectonics of the Northern Moine, NW Scotland. Ph.D. thesis, University of Leeds.

HOLDSWORTH, R.E. 1988. The stereographic analysis of facing. *Journal of Structural Geology*, **10**, 219–223.

HOLDSWORTH, R.E. 1989. The geology and structural evolution of a Caledonian fold and ductile thrust zone, Kyle of Tongue region, Sutherland, N. Scotland. *Journal of the Geological Society of London*, **146**, 809–823.

HOLDSWORTH, R.E. 1990. Progressive deformation structures associated with ductile thrusts in the Moine Nappe, Sutherland, N. Scotland. *Journal of Structural Geology*, **12**, 443–452.

HOLDSWORTH, R.E. & GRANT, C.J. 1990. Convergence-related 'dynamic spreading' in a mid-crustal ductile thrust zone: a possible orogenic wedge model. *In*: KNIPE, R.J. & RUTTER, E.H. (ed.) *Deformation mechanisms, rheology and tectonics* Geological Society, London, Special Publications, **54**, 491–500.

HOLDSWORTH, R.E. & ROBERTS, A.M. 1984. A study of early curvilinear fold structures and strain in the Moine of the Glen Garry region, Inverness-shire. *Journal of the Geological Society of London*, **141**, 327–338.

HOLDSWORTH, R.E., STRACHAN, R.A. & ALSOP, G.I. 2001. Geology of the Tongue District. *Memoirs of the British Geological Survey*. Sheet 114E (Scotland), 76 pp.

LACASSIN, R. & MATTAUER, M. 1985. Kilometre-scale sheath fold at Mattmark and implications for transport directions in the Alps. *Nature*, **315**, 739–742.

MIES, J.W. 1991. Planar dispersion of folds in ductile shear zones and kinematic interpretation of fold hinge girdles. *Journal of Structural Geology*, **13**, 281–297.

MINNIGH, L.D. 1979. Structural analysis of sheath-folds in a meta-chert from the Western Italian Alps. *Journal of Structural Geology*, **1**, 275–282.

PASSCHIER, C.W. 1997. The fabric attractor. *Journal of Structural Geology*, **19**, 113–127.

PLATT, J.P. 1983. Progressive refolding in ductile shear zones. *Journal of Structural Geology*, **5**, 619–622.

QUINQUIS, H., AUDREN, C., BRUN, J.P. & COBBOLD, P.R. 1978. Intense progressive shear in Ille de Groix blueschists and compatibility with subduction or obduction. *Nature*, **273**, 43–45.

RAMSAY, D.M. 1979. Analysis of rotation of folds during progressive deformation. *Geological Society of America Bulletin*, **90**, 732–738.

RAMSAY, J.G. 1967. *Folding and fracturing of rocks*. McGraw Hill.

RAMSAY, J.G. 1980. Shear zone geometry: a review. *Journal of Structural Geology*, **2**, 83–99.

RAMSAY, J.G. & HUBER, M. 1987. *The Techniques of Modern Structural Geology*. Volume 2: Folds and Fractures. Academic Press, London.

RAMSAY, J.G. & LISLE, R. 2000. *The techniques of modern structural geology*. Volume 3: Applications of continuum mechanics in structural geology. Academic Press, London.

RHODES, S. & GAYER, R.A. 1977. Non-cylindrical folds, linear structures in the X-direction and mylonite developed during translation of the Caledonian Kalak Nappe Complex of Finnmark. *Geological Magazine*, **114**, 329–341.

RIDLEY, J. 1986. Parallel stretching lineations and fold axes oblique to displacement direction-a model and observations. *Journal of Structural Geology*, **8**, 647–654.

SANDERSON, D.J. 1973. The development of fold axes oblique to the regional trend. *Tectonophysics*, **16**, 55–70.

SKJERNAA, L. 1989. Tubular folds and sheath folds: definitions and conceptual models for their development with examples from the Grapesvare area, northern Sweden. *Journal of Structural Geology*, **11**, 689–703.

TREAGUS, J.E. & TREAGUS, S.H. 1981. Folds and the strain ellipsoid: a general model. *Journal of Structural Geology*, **3**, 1–17.

WILLIAMS, G.D. 1978. Rotation of contemporary folds into the X direction during overthrust processes in Laksefjord, Finnmark. *Tectonophysics*, **48**, 29–40.